Butler-Craig *et al. Journal of Electric Propulsion* (2026) 5:44
https://doi.org/10.1007/s44205-026-00221-w

Journal of Electric Propulsion

RESEARCH Open Access

Characterization of a heaterless 60 A hollow cathode on krypton and argon

Naia Butler-Craig[1*], Dan Lev[1] and Mitchell L. R. Walker[1]

*Correspondence:
Naia Butler-Craig
naiabc3@gatech.edu
[1]Georgia Institute of Technology, Atlanta, USA

Abstract

We present a steady-state current-voltage (IV) characterization of a heaterless version of the 9 kW-class H9 Hall thruster cathode. This work was conducted at Georgia Tech's High-Power Electric Propulsion Laboratory (HPEPL) at operational background pressures of 0.22–0.70 µTorr on krypton and 0.11–0.24 µTorr on argon, with a base pressure of 9.1×10^{-8} Torr. The characterization mapped steady-state voltage behavior from 5 to 45 A of discharge current on krypton and 5 to 30 A on argon (with paired magnetized and unmagnetized data over 5 to 35 A on krypton and 5 to 20 A on argon), in both magnetized and unmagnetized configurations. The magnetized configuration produced a higher discharge voltage than the unmagnetized configuration at every paired (current, flow) operating point on both propellants. On krypton, the magnetized-unmagnetized voltage gap ranged from near zero at the highest cathode flow and lowest current to +39.6 V (+148%) at 30 A and 12.39 sccm. On argon, the gap ranged from +6.0 V at 15 A and 12.39 sccm to +67.5 V (+159%) at 20 A and 15.89 sccm. In both cases, the gap widened with discharge current and narrowed with cathode flow. These results verify reproducible ignition at every tested flow rate, confirm uninterrupted steady-state heaterless operation on krypton and argon, and quantify how the applied magnetic field shifts the steady-state operating point at fixed discharge current. The key finding is that the applied magnetic field increases the steady-state discharge voltage at fixed current rather than reducing it, and the effect is systematically larger on argon than on krypton at matched operating conditions.

Keywords Heaterless hollow cathode, Hall thruster, Electric propulsion, Krypton, Argon, Magnetized cathode, Paschen breakdown

Introduction

Hollow cathodes are critical components in electric propulsion systems, serving as electron sources for propellant ionization and plume neutralization in Hall effect thrusters [1]. Conventional hollow cathodes typically require an external heater to raise the thermionic emitter to emission temperatures, which adds complexity to the system, increases power consumption, and introduces a potential failure point due to thermal cycling of the heater assembly. Heaterless hollow cathodes eliminate the need for an external heater by utilizing a high-voltage Paschen discharge between the cathode and keeper electrodes to heat the emitter to operational temperatures [2].

Recent work has significantly advanced heaterless hollow cathode technology. Payman and Goebel (2022) [3] demonstrated a breakthrough in scaling heaterless cathodes to higher currents with their High Emission Current Cathode with Tube-Radiator (HECCTR) design. By extending a refractory metal tube into the insert region, they achieved stable operation at 50 A while avoiding the arcing and inefficient heating that limited previous high-current attempts. This design was subsequently scaled to 300 A operation [4], demonstrating the viability of heaterless cathodes for high-power Hall thrusters. Previous literature has highlighted the importance of understanding time-resolved ignition characteristics in heaterless cathodes. Lev et al. (2017) conducted a comprehensive review of heaterless technology, emphasizing that the transition from initial Paschen breakdown to steady-state thermionic emission is critical for cathode longevity [5]. The ignition process in HHCs occurs in distinct phases, with the three main stages being breakdown, heating, and steady-state operation [6]. It has been shown by various experiments that the transition between these phases is critical, with the breakdown voltage being heavily influenced by geometric parameters and pressure conditions [7].

While significant progress has been made in developing high-current (> 50 A) heaterless hollow cathodes operating on xenon, relatively little work has been done to characterize their performance with alternative propellants such as krypton and argon. These propellants are of interest for Hall thrusters due to their lower cost compared to xenon. However, they typically require higher discharge voltages and power to achieve similar levels of ionization. Prior Hall-thruster performance studies have further reported 5–10% lower propellant utilization and approximately 8% wider beam divergence on krypton than on xenon, which together account for most of the reported krypton-xenon efficiency gap [8]. The behavior of heaterless hollow cathodes with these propellants merits investigation, as the different ionization potentials and atomic masses affect both the initial Paschen breakdown characteristics and the subsequent heating of the thermionic emitter. While prior work by Daykin-Iliopoulos et al. (2019) characterized HHC operation up to 30 A with krypton and argon propellants, demonstrating differences in electron density and temperature profiles between propellants, the effects of magnetic fields remained unexplored. Their work showed that krypton exhibited a higher initial electron density ($\sim 2.4 \times 10^{20}$ m^{-3}) than argon ($\sim 1 \times 10^{20}$ m^{-3}), and that argon required higher operating temperatures due to its higher ionization potential [9]. Beyond steady-state impedance, the keeper-voltage spectrum is a diagnostic of cathode operating state: elevated peak-to-peak keeper voltage has been identified as an indicator of transition to plume-mode operation [10]. The flow rate and discharge-current regimes that produce plume-mode oscillations on krypton and argon have not been mapped in the heaterless hollow cathode literature. The present work builds upon this foundation by investigating the previously unexplored impact of magnetization on discharge characteristics with these alternative propellants. Through frequency analysis of steady-state operation under both magnetized and unmagnetized conditions, this study provides new insights into how magnetic fields influence HHC operation with krypton and argon propellants. In magnetized cathode plumes coupled to Hall-effect thrusters, coherent instability activity, including ion acoustic turbulence and azimuthal anti-drift modes, has been associated with enhanced electron collisionality [11]. The standalone, mock-H9-magnetized configuration examined here differs from that coupled-thruster geometry, which motivates direct measurement of the keeper-voltage spectrum on both propellants in the present work.

This paper presents the characterization of a heaterless hollow cathode based on modifying the centrally mounted LaB6 cathode of the H9 magnetically shielded Hall thruster developed at the University of Michigan. The H9's original cathode design was adapted to the recent HECCTR concept, in which a refractory metal tube partially extends the gas feed line into the insert region. This novel configuration prevents the inefficient coupling of the high-voltage discharge to upstream components that plagued earlier heaterless cathode attempts. The experimental campaign examines the time-resolved current-voltage characteristics during startup, providing insight into the ignition dynamics for both krypton and argon. Additionally, the steady-state performance is evaluated through anode voltage-current characteristics at three different mass flow rates, under both magnetized and unmagnetized conditions. Particular attention is paid to time-resolved ignition characteristics and the effects of magnetization on discharge behavior. Together, these measurements provide a characterization of the modified heaterless H9 cathode on krypton and argon under both magnetized and unmagnetized conditions.

Experimental set-up

Section "Test facilities" describes the vacuum test facility in which the experiment was conducted, along with the diagnostic instruments and data acquisition methods used to capture time-resolved cathode telemetry. Section "Heaterless hollow cathode and operating conditions" presents the heaterless hollow cathode design and operating conditions. Finally, Section "Ignition procedure" presents the ignition sequence for cathode start-up.

Test facilities

High-Power Electric Propulsion Laboratory Vacuum Test Facility 2

The experiment was carried out in Vacuum Test Facility 2 (VTF-2) at Georgia Tech's High Power-Electric Propulsion Laboratory (HPEPL). VTF-2 is a stainless-steel chamber that measures 9.2 m in length and 4.9 m in diameter. The chamber is then evacuated to a moderate vacuum of approximately 10 mTorr, measured with an Agilent Varian 531 Thermocouple Vacuum gauge. This rough vacuum was achieved through one 3800 CFM blower and one 495 CFM rotary-vane pump. To reach high vacuum, the facility utilizes 10 LN_2-cooled CVI TMI reentrant cryopumps that provide a pumping speed of approximately 400,000 L/s on krypton. The pressure in the high-vacuum phase of operation is measured in three locations: two internal and one externally mounted on a chamber flange. All three locations employ an Agilent Bayard-Alpert 571 hot-filament ion gauge. The ion-gauge readings were corrected for krypton and argon using the manufacturer gas correction factors, so the operational pressures in Tables 1 and 2 are gas-corrected partial pressures. Averaging over the three measurements provides a base pressure of 9.1×10^{-8} Torr, and the operational pressures for krypton and argon can be found in Tables 1 and 2, respectively.

In this setup, the cathode is mounted in the inner bore of the H9 Hall thruster. Because of this, the inner and outer coils in the thruster simulate the magnetic field and

Table 1 Krypton characterization operating conditions

I_D (A)	Flow Rate	Operational Pressure (μTorr-Kr)	Rationale
5, 6, 7.5, 10, 15, 20, 25, 30 (M, U); 35, 40, 45 (U only)	0.77 mg/s (12.4 sccm)	0.26–0.38	7% CFF 15 A, 4.5 kW Kr
5, 6, 7.5, 10, 15, 20, 25, 30 (M, U); 35, 40, 45 (U only)	0.99 mg/s (15.9 sccm)	0.27–0.33	7% CFF 20 A, 6 kW Kr
5, 6, 7.5, 10, 15, 20, 25, 30 (M, U); 35, 40, 45 (U only)	1.40 mg/s (22.3 sccm)	0.51–0.58	7% CFF 30 A, 9 kW Kr

Table 2 Argon characterization cathode operating conditions

I_D (A)	Flow Rate	Operational Pressure (μTorr-Ar)	Rationale
5, 6, 7.5, 10, 15	0.37 mg/s (12.4 sccm)	0.11–0.13	Match Kr volumetric flow rate
5, 6, 7.5, 10, 15, 20 (M, U); 25, 30 (U only)	0.47 mg/s (15.9 sccm)	0.13–0.18	Match Kr volumetric flow rate
5, 6, 7.5, 10, 15 (M, U); 20, 25, 30 (U only)	0.66 mg/s (22.3 sccm)	0.21–0.24	Match Kr volumetric flow rate

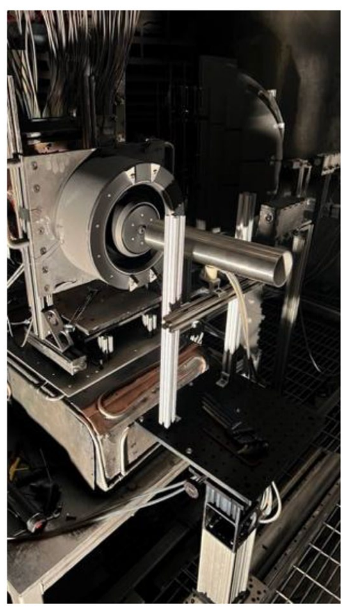

Fig. 1 H9 Cathode with external anode experimental setup in VTF-2

are set to match the nominal magnetic field strength when running nominally. Figure 1 depicts the cathode mounted in the H9 Hall thruster with the stainless-steel external anode mounted 30.5 mm downstream of the cathode keeper face. The external anode is a 305 mm-long cylinder with a 56.9 mm diameter. Throughout the characterization the inner and outer magnet coils were held at fixed currents of 4.11 A (inner) and 2.27 A (outer) for the magnetized cases, producing a keeper-region field of approximately 175 G on krypton and 150 G on argon as read on the centerline field channel; the two values reflect the field read for each propellant campaign at the same coil settings. The unmagnetized cases were run with both coils at zero current (0 G).

The cathode circuit for this experiment can be found in Fig. 2. As shown in the circuit, the anode discharge is powered by a 150 V, 100 A TDK-Lambda GEN150-100 power supply. The inner and outer magnet solenoids are powered by TDK-Lambda GEN40-38 (40 V, 38 A) and GEN80-42 (80 V, 42 A) power supplies, respectively. The keeper current and voltage are supplied by two diode-added supplies in parallel. The first is a 1000 V, 1.5 A Magna-Power SLC1000-1.5/UI DC power supply needed to deliver 1 kV to the cathode for the initial breakdown. The second is a 600 V, 2.6 A TDK Lambda GEN600-2.6 power supply for the keeper current to sustain thermionic emission on the LaB_6 insert. The keeper discharge filter adds two 50-Ω resistors, and a 10-mH inductor in series to limit both current and voltage oscillations due to keeper discharge instabilities on ignition. The cathode is supplied with research-grade krypton and argon via an MKS GE50A digital mass flow controller. The MFC was calibrated on both gases at the test article using a MesaLabs DryCal 800 – 10 volumetric flow meter, and a linear fit was generated between the commanded and measured flow rates. Flow calibrations on krypton showed a maximum error of 3% while flow calibrations on argon showed a maximum error of 8%. Combining the discharge-supply readback calibration (0.4% of reading) with the reading resolution gives a steady-state discharge-voltage uncertainty of approximately ± 0.5% (for example, ± 0.2 V at 30 V and ± 0.6 V at 110 V). Propagating this through the magnetized-minus-unmagnetized voltage difference gives an uncertainty of approximately ± 0.4 V on the krypton voltage gap and ± 0.6 V on the argon voltage gap at the operating points reported below. Time-resolved cathode telemetry was measured with a Teledyne LeCroy HDO6104 oscilloscope with a 10 MS/s sampling rate. The keeper voltage was measured with a Powertek DP25 differential voltage probe rated up to 25 MHz, while the keeper current was measured with a Teledyne LeCroy CP150 current clamp. The steady-state discharge voltage and current reported in Section "Steady-state operation" and "Frequency analysis" were taken from the front-panel

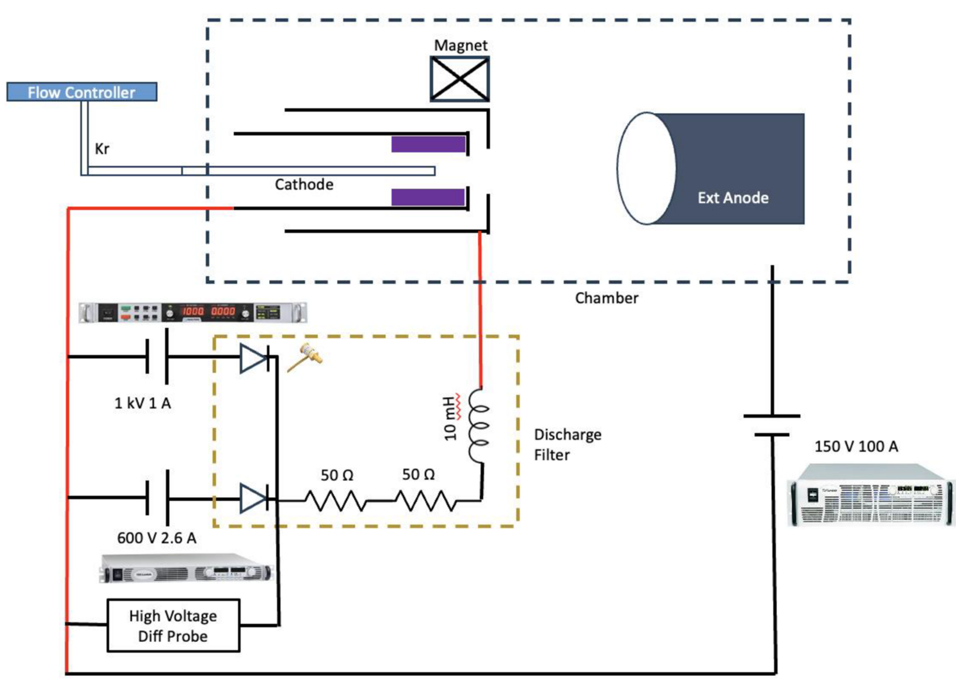

Fig. 2 Cathode circuit electrical schematic

readback of the TDK-Lambda GEN150-100 discharge supply after the discharge voltage and current had stabilized at each operating point. The discharge-supply readback was calibrated against a bench digital multimeter over the full operating range; the readback agreed with the multimeter to within 0.4% of reading, which bounds the systematic voltage uncertainty. Each tabulated point is a single steady-state reading rather than an average of repeated sweeps.

Heaterless hollow cathode and operating conditions

The study was performed on the cathode developed for the H9, a 9-kW class magnetically shielded HET developed by the Jet Propulsion Laboratory in collaboration with the University of Michigan and the Air Force Research Laboratory [12]. Figure 3 shows the Adapted H9 Cathode Heaterless Design Schematic. The thruster body was used as a mounting structure. The cathode is based on the compact lanthanum hexaboride hollow cathode design developed at JPL for centerline mounting in Hall thrusters, which is rated for emission currents up to 60 A [13]. The original H9 design was modified to be heaterless by implementing the HECCTR design outlined in Ref [3]. The modified H9 employs a 3.3 mm diameter Tantalum (Ta) tube internal to the hollow cathode that protrudes 12.7 mm into the hollow insert to radiatively heat it internally. This contrasts with the sheathed heater cable coiled around the cathode body in the original design.

The cathode was characterized on krypton at the operating conditions shown in Table 1 for both the magnetized and unmagnetized cases. Cathode flow rates were selected to match the cathode flow rate when running nominally in the H9 thruster on krypton with a 7% cathode flow fraction at the three nominal thruster operating conditions: 4.5 kW, 6 kW, and 9 kW. The flow rate in each row was held fixed during the current sweep; the 7% cathode flow fraction applies at the nominal thruster discharge current of the listed operating condition. An additional sweep with the cathode flow scaled to discharge current at 0.7 sccm/A (10 to 24.5 sccm) was also performed. In Tables 1 and 2, (M) and (U) denote the magnetized and unmagnetized configurations; currents marked (U only) were achieved only without the applied field, as magnetized operation was limited by anode thermal loading on krypton and by the 150 V discharge supply compliance on argon.

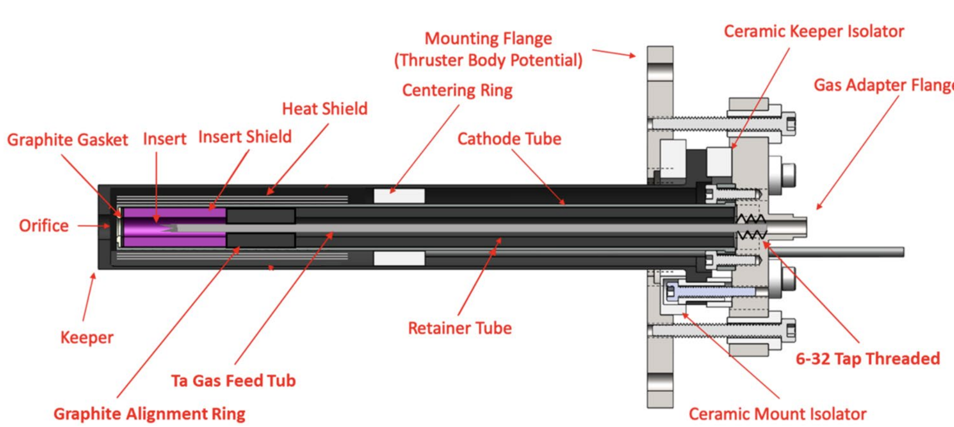

Fig. 3 Adapted H9 Cathode Heaterless Design Schematic

The cathode was characterized on argon at the operating conditions shown in Table 2 for both the magnetized and unmagnetized cases. The cathode flow rates were selected to match the cathode flow rates for krypton characterization listed in Table 1.

Ignition procedure

The cathode conditioning and ignition procedures were the same throughout this study. As mentioned in Ref. [5], a heaterless cathode usually transitions through three heating modes before ignition on an anode for the main discharge. In this design, those three modes are: high-voltage Paschen breakdown that heats the Ta inner tube, the intermediate-voltage thermionic discharge from the Ta inner tube that radiatively heats the LaB_6 insert, and finally, the low-voltage LaB_6 thermionic discharge from the insert. The heating transitions are initiated by slowly and stably increasing the keeper current. When the LaB_6 is sufficiently hot for thermionic discharge, the cathode becomes self-heating at an anode current greater than 6 A. Below this anode current, a small keeper current of approximately 100 mA is necessary to sustain the anode discharge; otherwise, the cathode will shut itself off.

The chronological steps for cathode ignition are [6, 7]:

1. **High-Voltage Paschen Breakdown**: An elevated propellant flow is supplied to the cathode; here, the flow required for ignition is defined as the lowest cold-flow rate at which the discharge transitions to a sustained arc rather than repeatedly extinguishing. By this definition, a conditioned cathode ignited on krypton at 72 sccm, whereas a cold cathode produced no sustained breakdown below 110 sccm (Section "Ignition profiles"). The high-voltage keeper supply is then turned on to initiate Paschen breakdown at a setpoint of approximately 1 kV, current-limited at 0.25 A. After the breakdown, the keeper voltage naturally falls to the Paschen minimum, which is dependent on the propellant but is usually about 200–250 V.
2. **Intermediate-Voltage Thermionic Ta Discharge**: When this voltage is stable, the keeper current is slowly increased to 1.5 A, the limit on the high-voltage supply. At this point, the keeper voltage should drop to less than 45 V to indicate the transition to thermionic discharge on the Ta inner tube.
3. **Low-Voltage LaB6 Thermionic Discharge**: From this point, the keeper current is increased to 2.6 A, which was found to be the minimum current to sustain a thermionic discharge on the LaB6 insert. At this stage, the keeper voltage should drop below 20 V to indicate a successful transition to this self-heating mode on the insert.

Figure 4 shows a representative transition between the cathode heating modes, keeper voltage as a function of time. The trace illustrates the three-stage ignition sequence used throughout this study: an initial high-voltage Paschen breakdown phase in which the keeper supply drives the cathode-to-keeper gap until impact-ionization avalanche initiates a discharge, a tantalum thermionic phase in which the keeper voltage settles to an intermediate level as the Ta tube heats and begins supplying electrons, and a final LaB_6 thermionic phase in which the keeper voltage drops below 20 V as the insert reaches emission temperature. Figure 4 is included here to anchor the procedure described above to a real voltage waveform, so that the reader can associate each numbered step in the procedure with the corresponding segment of the keeper-voltage trace. The specific voltage magnitudes and transition times shown here are representative only; the

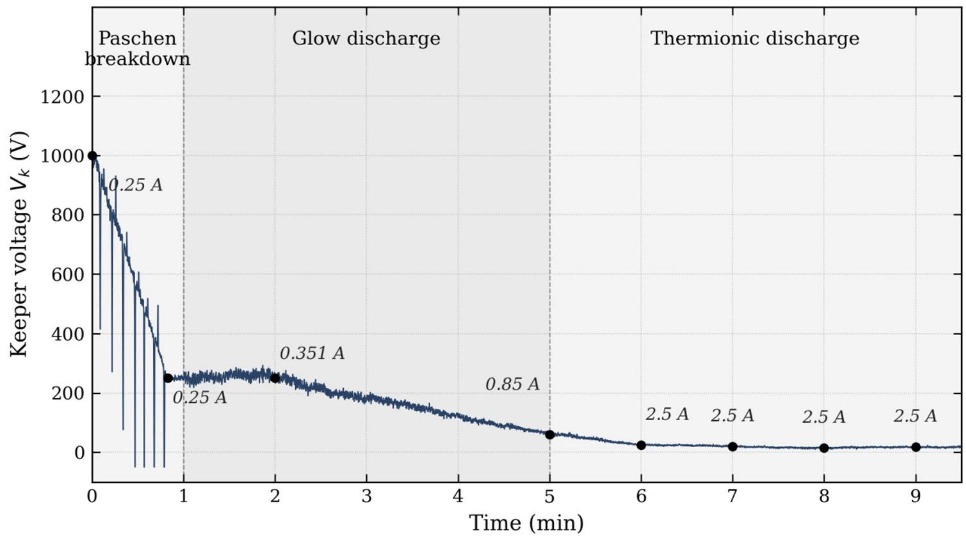

Fig. 4 Example cathode ignition

quantitative ignition behavior for krypton and argon is presented in the Results section. The vertical excursions visible in the Paschen-discharge region of Fig. 4 correspond to repeated breakdown and extinction events during the high-voltage heating phase. These events appeared on every ignition and are a characteristic feature of the Paschen-regime conditioning of the tantalum tube-radiator; consistent with the behavior reported for the HECCTR reference design [3], they occur on the refractory tantalum tube rather than the LaB6 insert, and post-test inspection showed no damage to either the tube or the insert.

Results

This section presents the experimental results from the heaterless hollow cathode characterization at Georgia Tech's HPEPL facility. The ignition profiles for both propellants are presented first, followed by the steady-state voltage-current characteristics under magnetized and unmagnetized conditions across three flow rates. Frequency analysis of the discharge oscillations is then presented for both propellants. The ignition behavior reported in Section "Ignition profiles" reflects the heaterless startup sequence and is governed by breakdown physics. The steady-state characteristics in Section "Steady-state operation" and "Frequency analysis" describe the thermionic discharge after heating is complete and are largely independent of the ignition path.

Figure 5 shows the heaterless H9 cathode in steady-state operation on krypton at two discharge currents, 30 A on the left and 15 A on the right. In both cases, the plume is centered on the keeper orifice, consistent with on-axis emission, and the higher-current condition produces a visibly brighter and more radially extended plume as expected from the larger total electron emission and the higher local ion-production rate. These images document the physical state of the cathode during the steady-state characterization that follows and provide a visual confirmation that the cathode operated stably across the current envelope investigated in this study.

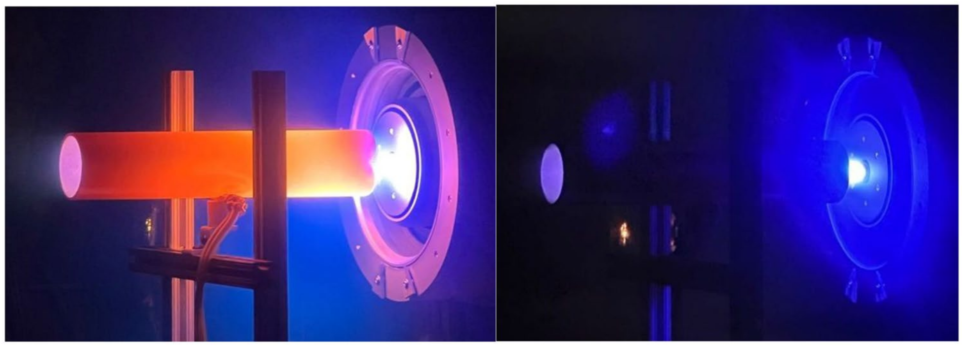

Fig. 5 Cathode operating on krypton at 30 A (left) and 15 A (right)

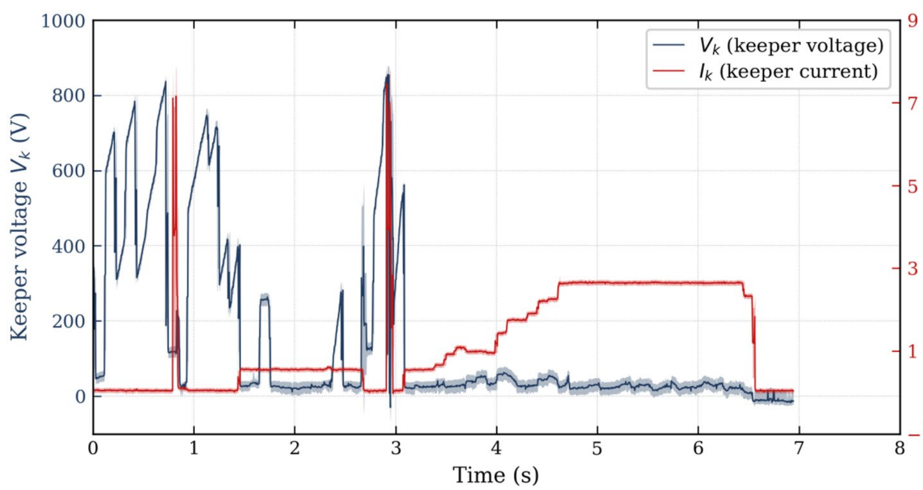

Fig. 6 Cathode ignition profile – keeper voltage and keeper current as a function of time for a flow rate of 150 sccm krypton

Ignition profiles

Understanding ignition profiles is critical for both cathode design and reliable operation. As highlighted by Ref. [6], the transition between ignition phases (breakdown, heating, steady-state) is crucial for cathode longevity, as improper transitions can lead to destructive arcing and damage. The time-resolved behavior provides insight into the physical mechanisms governing startup and stable operation, which is particularly important for heaterless designs where conventional heating methods aren't available. Moreover, different propellants exhibit distinct ignition characteristics that influence key design parameters such as keeper geometry, gas flow requirements, and power supply specifications. For spacecraft applications, where fast and reliable ignition is essential, detailed characterization of these ignition profiles across different operating conditions enables the development of robust startup procedures and more reliable high-current cathodes.

The ignition plots shown in Fig. 6 demonstrate repeated attempts at a Paschen breakdown at a measured peak keeper voltage of approximately 800 V (with the supply set to 1 kV); because this trace is the 150 sccm ignition, its breakdown peak sits near the low-flow-end value of Fig. 8 rather than the ~905 V typical of lower flows until ignition occurs at approximately 3 min, with the keeper current limited to 0.25 A. The trace shown corresponds to an elevated-flow ignition at 150 sccm, selected as a representative clean breakdown; routine krypton ignition on a conditioned cathode occurred at

72 sccm. The transition to thermionic discharge on the Ta tube is evident as the voltage drops to around 40–45 V, showing effective heating of the internal Ta tube. The voltage spikes during the initial Paschen breakdown phase show characteristic relaxation oscillations, where the voltage rapidly rises to breakdown level (~800 V), then quickly drops as the discharge occurs, creating a sawtooth pattern. These oscillations persist until sufficient heating of the tantalum tube is achieved, which enables a more stable discharge with reduced voltage oscillations. Based on the timescale shown in the figure, the frequency of these oscillations appears to be in the Hz range, and their amplitude gradually decreases as the cathode transitions from the high-voltage Paschen breakdown mode to the intermediate-voltage tantalum thermionic mode. The transition to LaB_6 thermionic emission shows distinct voltage and current behavior, with the keeper voltage exhibiting smaller amplitude oscillations compared to the initial Paschen breakdown phase. As the keeper current is increased to 2.6 A, the voltage shows a series of step-like reductions, with brief oscillations at each step, indicating the gradual heating of the LaB_6 insert to the emission temperature. The final stabilization below 20 V shows minimal oscillations, suggesting achievement of uniform thermionic emission across the LaB_6 surface. These more stable oscillation patterns during the LaB_6 transition, compared to the violent spikes during Paschen breakdown, indicate a more controlled heating process facilitated by the tantalum tube's radiative heating of the insert.

The character of these oscillations depends on the ignition flow rate. Figure 7 shows Paschen-stage keeper voltage and current captures on krypton at six cold-flow rates from 100 to 150 sccm, and Fig. 8 summarizes the observed breakdown voltage across these flows. For each capture, the breakdown voltage is taken as the peak keeper voltage reached prior to current onset, read directly from the upper edge of the digitized

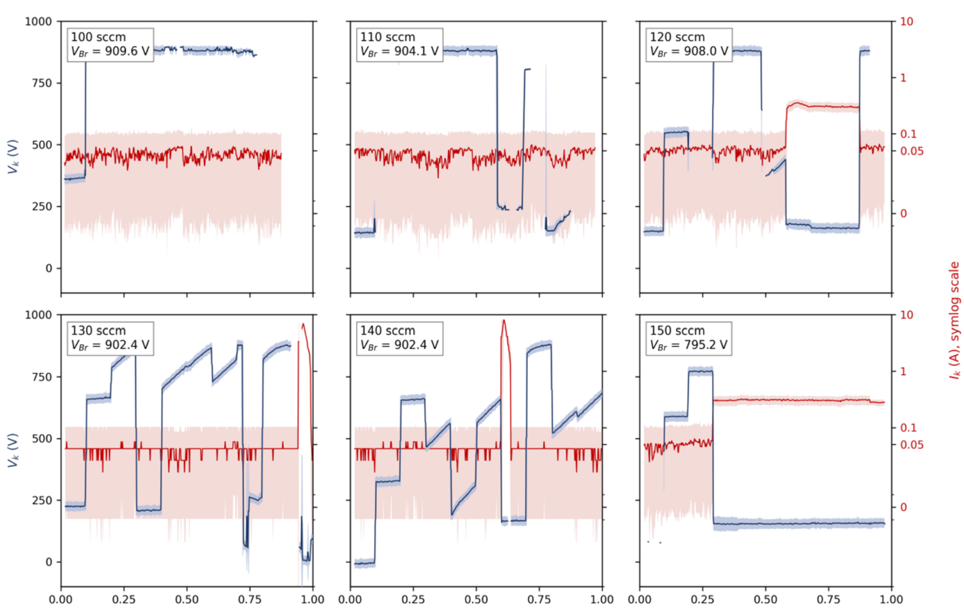

Fig. 7 Krypton Paschen breakdown keeper voltage and keeper current captures at six cold-flow rates (100, 110, 120, 130, 140, and 150 sccm). Each panel shows V_k (navy, left axis) and I_k (red, right axis) over the breakdown window, with the 15th to 85th percentile envelope shaded and the median plotted as a thin centerline. The extracted breakdown voltage V_{Br} is annotated in each panel. All panels share a common voltage axis (0 to 1000 V) and a common symlog keeper-current axis to permit direct comparison across flows. The red curve is the midline of the keeper-current envelope (shaded); because the current axis is symlog, this midline does not coincide with the visual center of the shaded band

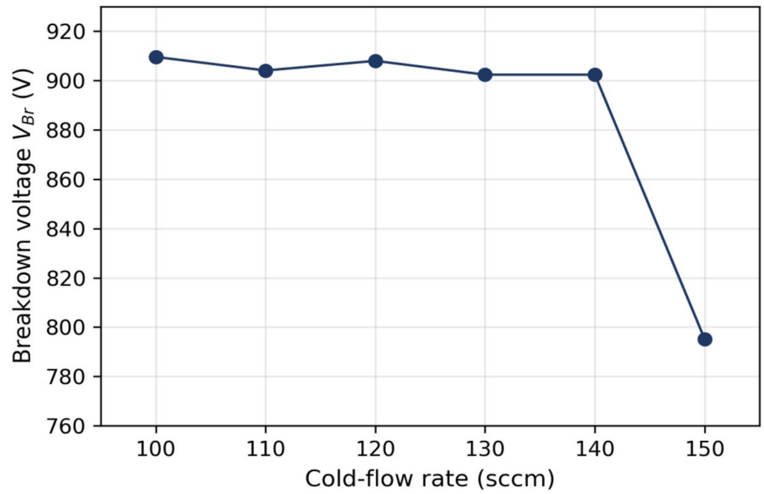

Fig. 8 Observed keeper breakdown voltage as a function of cold-flow rate on krypton. For each flow, the breakdown voltage is defined as the peak keeper voltage recorded prior to current onset, read from the upper edge of the digitized keeper-voltage envelope. The same method is applied to all six captures

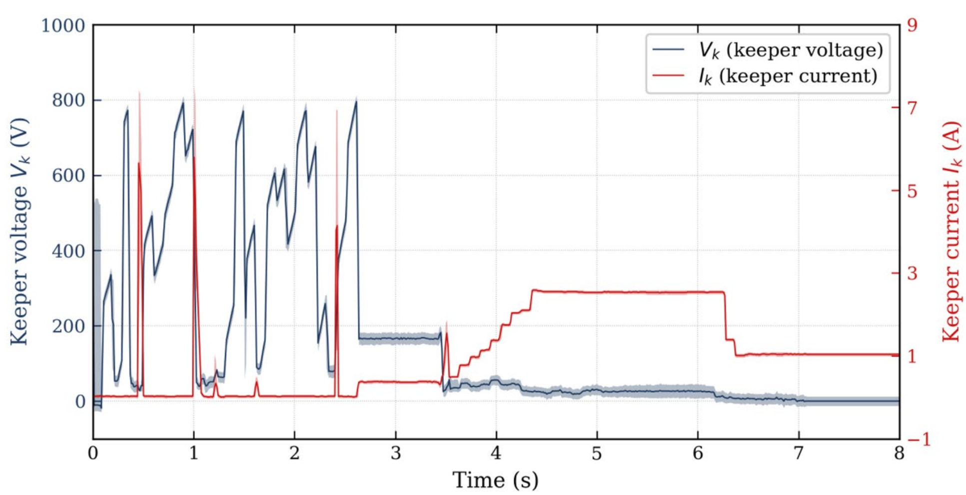

Fig. 9 Argon ignition profile with a flow rate of 140 sccm: Keeper voltage and keeper current as a function of time

keeper-voltage envelope, so that every reported value reflects the same physical definition and the same measurement method. Between 100 and 140 sccm, the breakdown voltage is nearly flat near 905 V (ranging from 902 to 910 V), with the breakdown character evolving from persistent pre-breakdown chatter at the lower flows to discrete stair-step breakdown attempts terminating in a full arc transition at 130 and 140 sccm. At 150 sccm, the breakdown voltage drops sharply to approximately 795 V, and the cathode transitions cleanly into sustained arc operation. This behavior is consistent with the cathode operating on the low-pressure branch of the Paschen curve, where the breakdown voltage decreases toward the Paschen minimum as the insert neutral density rises with flow.

As evidenced by Fig. 9, argon exhibits higher operating voltages during all three stages of ignition compared to krypton, which aligns with its higher ionization potential, 15.76 eV for argon and 14.0 eV for krypton. Both propellants show a successful transition through the three characteristic stages, beginning with Paschen breakdown at approximately 800 V, followed by tantalum thermionic emission, and culminating in LaB_6 thermionic emission at keeper voltages below 20 V. Successful Paschen breakdown appears to occur at approximately 2.6 min with very clean transitions to the subsequent heating phases. Argon was much more difficult to ignite and necessitated an initial flow rate of 140 sccm, far exceeding that of krypton, so its breakdown peak likewise reflects an elevated-flow ignition.

Steady-state operation

The steady-state voltage-current (IV) characteristics of the heaterless hollow cathode provide critical information about its operational efficiency and stability across different discharge conditions. Steady-state operation was confirmed when the discharge voltage and current had stabilized and were no longer drifting, consistent with the cathode reaching thermal equilibrium. The plots show the relationship between anode voltage and discharge current, with higher voltages indicating greater power requirements to maintain the desired discharge current. For both krypton and argon operation, data were collected at three different flow rates under both magnetized and unmagnetized conditions, with discharge currents ranging from 5 to 45 A on krypton (up to 30 A magnetized at the fixed flow rates and 35 A on the flow-scaled sweep) and 5 to 30 A on argon (up to 20 A magnetized). Figure 10 shows the steady-state IV characteristics for krypton. In the examination of both gases, if the plot does not show the full current sweep up to the maximum current attempted at that condition, that is either because (1) the anode appeared too hot to continue operating at the discharge condition safely, or (2) the voltage required to sustain the anode discharge exceeded the power supply's capabilities. These issues became prevalent in the magnetized cases of both gases, but especially in argon, as it was very unstable at high currents.

Figures 10 and 11 show that the magnetized case consistently produces a higher discharge voltage than the unmagnetized case on both propellants at every paired operating point. Across the 30 paired krypton conditions (discharge current 5 to 35 A, cathode flow 10 to 24.5 sccm), the magnetized-unmagnetized voltage difference ranges from near zero at the highest flow and lowest current to + 39.6 V (+ 148%) at 30 A and 12.39 sccm. Across the 16 paired argon conditions (discharge current 5 to 20 A, cathode flow 12.39 to 22.33 sccm), the voltage difference ranges from + 6.0 V at 15 A and 12.39 sccm

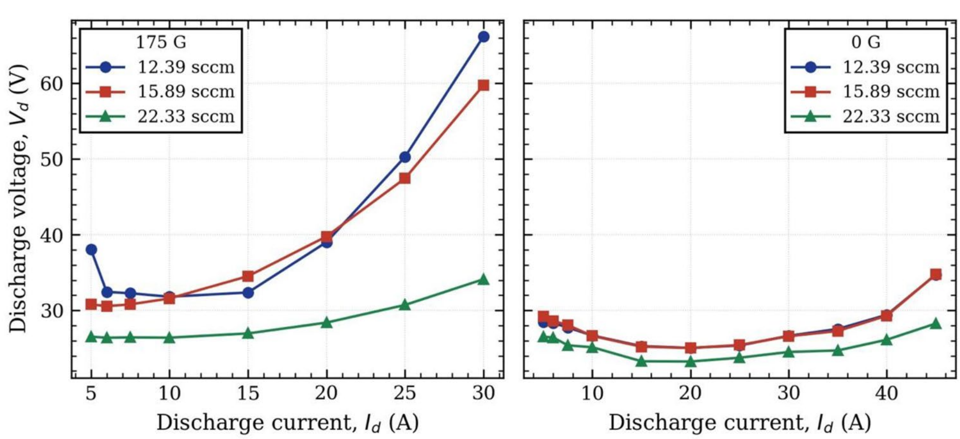

Fig. 10 Discharge voltage as a function of discharge current for steady-state operation on krypton in the unmagnetized (U) and magnetized (M) configurations for flow rates of 12.39, 15.89, and 22.33 sccm

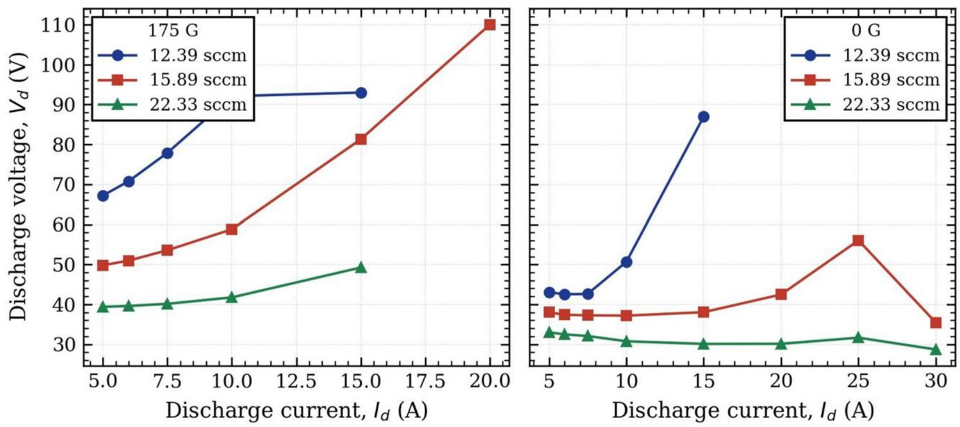

Fig. 11 Argon steady-state IV characteristic in the unmagnetized (U) and magnetized (M) cases

to + 67.5 V (+ 159%) at 20 A and 15.89 sccm. For both propellants, the voltage gap widens as discharge current increases and narrows as cathode flow increases, so the largest shifts occur at the lowest flow and highest current. The test operator also visually noted that the stainless-steel anode began to glow yellow, indicating incandescence at an approximate surface temperature of 1000 to 1100 °C [14].

The magnetic-field effect is more pronounced on argon than on krypton at matched operating conditions, comparing Figs. 10 and 11. For example, at 10 A and 15.89 sccm, the magnetized-unmagnetized discharge-voltage gap is +4.9 V on krypton versus +21.6 V on argon; across the paired conditions where both propellants were run, the argon gap is typically three to eight times the krypton gap in absolute volts.

Frequency analysis

This section reports the power spectral density of the cathode keeper voltage across the krypton and argon operating envelopes, with attention to how cathode flow rate, discharge current, and keeper-region magnetization shape the keeper-voltage spectrum. Peak-to-peak keeper voltage has previously been identified as an indicator of oscillation level in the cathode plume, with elevated values associated with transition to plume-mode operation [10]. In magnetized cathode plumes coupled to Hall-effect thrusters, coherent instability activity in the cathode plume, including ion acoustic turbulence and azimuthal anti-drift modes, has been associated with enhanced electron collisionality [11]; the standalone, mock-H9-magnetized configuration used here differs from that coupled-thruster geometry, and the literature is cited as context for the frequency content reported below rather than as a direct comparison. Four figures are presented. Figures 12 and 15 compare magnetized and unmagnetized operation at a fixed discharge current for krypton and argon, respectively, isolating the effect of the applied magnetic field. Figures 13 and 14 resolve the magnetized condition across the discharge-current sweep at three cathode flow rates, enabling comparison of how the spectrum scales with discharge current and flow rate on the two propellants. A dedicated no-plasma baseline capture was not recorded during the campaign. The noise floor of the measurement chain (HDO6104 oscilloscope at 10 MS/s, DP25 differential voltage probe, CP150 current clamp) is assessed from the flat, featureless high-frequency floor of breakdown-phase spectra acquired with the same chain, which sits near − 90 dB/Hz and below; the

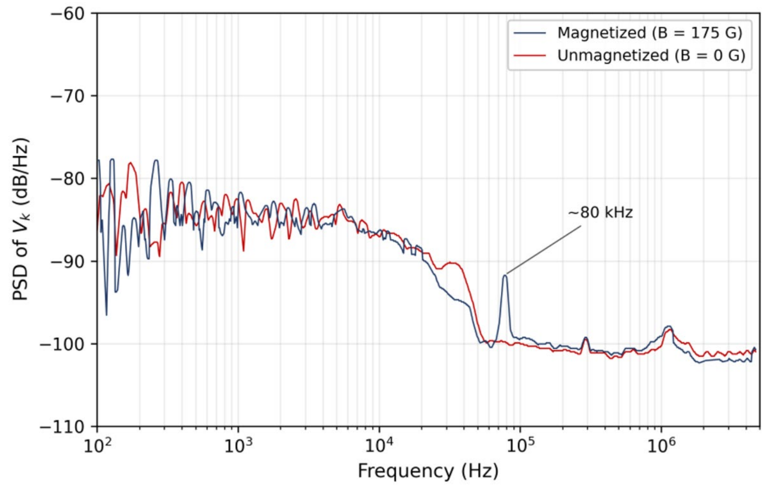

Fig. 12 Krypton keeper voltage power spectral density at I_d = 20 A and 22.33 sccm cathode flow, log-bin averaged. Blue trace: magnetized case (B = 175 G, orifice coil current OC = 2.27 A). Red trace: unmagnetized case (B = 0 G)

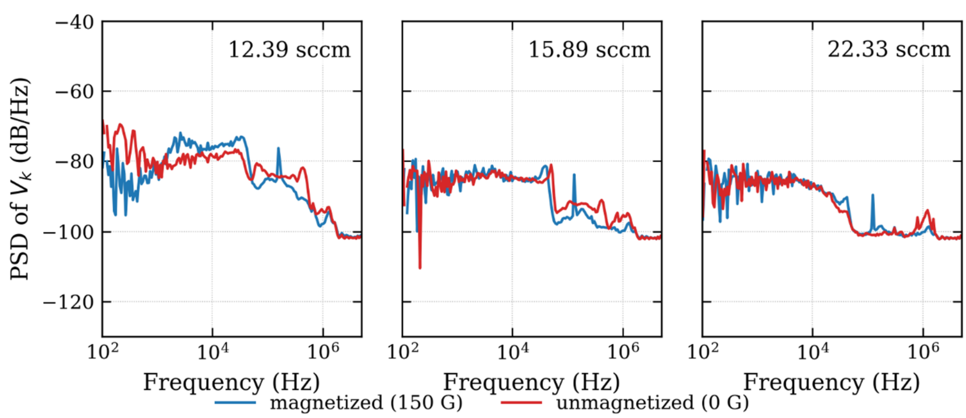

Fig. 15 Argon keeper voltage power spectral density at I_d = 10 A, log-bin averaged. Three panels, one per cathode flow rate: 12.39 sccm (left), 15.89 sccm (center), 22.33 sccm (right). Each panel overlays the magnetized case (B = 150 G, OC = 2.27 A, blue) and the unmagnetized case (B = 0 G, red)

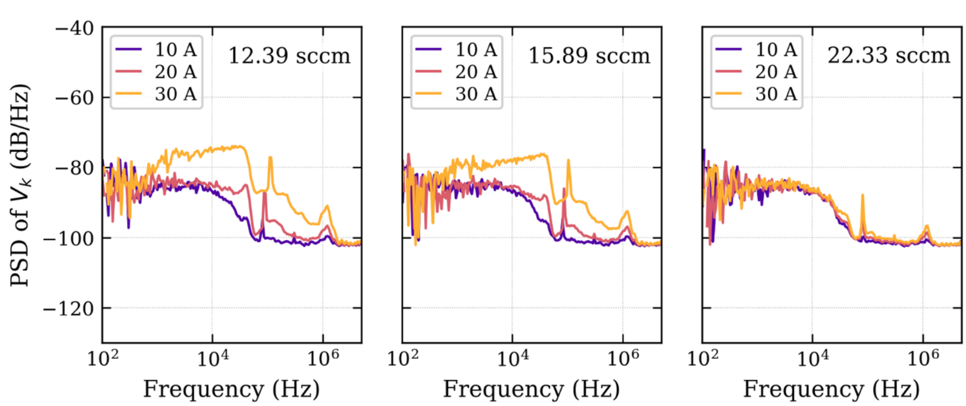

Fig. 13 Krypton keeper voltage power spectral density at B = 175 G (OC = 2.27 A), log-bin averaged. Three panels, one per cathode flow rate: 12.39 sccm (left), 15.89 sccm (center), 22.33 sccm (right). Each panel overlays traces at discharge currents I_d = 10, 20, and 30 A, colored from dark purple (low current) through orange to yellow (high current) on the plasma colormap

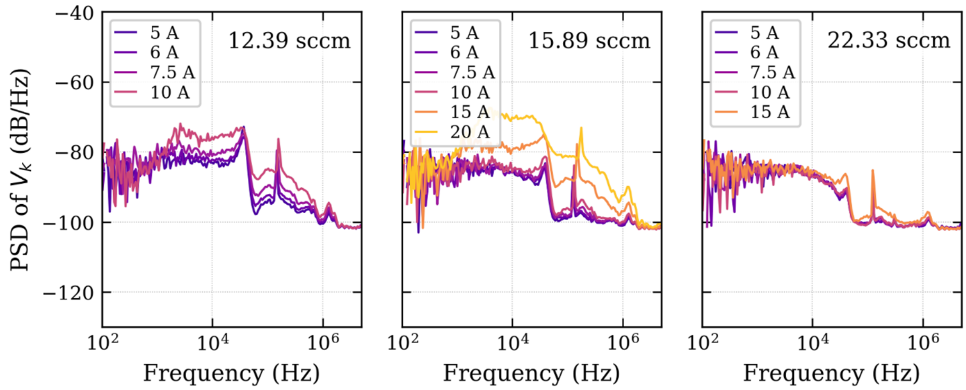

Fig. 14 Argon keeper voltage power spectral density at B = 150 G (OC = 2.27 A), log-bin averaged. Three panels, one per cathode flow rate: 12.39 sccm (left), 15.89 sccm (center), 22.33 sccm (right). Each panel overlays traces at discharge currents colored from dark purple (low current) through orange to yellow (high current) on the plasma colormap. The 12.39 sccm panel contains I_d = 5, 6, 7.5, and 10 A; the 15.89 sccm panel contains I_d = 5, 6, 7.5, 10, 15, and 20 A; the 22.33 sccm panel contains I_d = 5, 6, 7.5, 10, and 15 A

coherent spectral features reported in Figs. 12 through 15 rise well above this level, and the floor contributes no coherent peaks in the band of interest.

Figure 12 compares the krypton keeper voltage power spectral density at a single operating point, a discharge current of 20 A and 22.33 sccm, for the magnetized and unmagnetized configurations. This pairing holds the operating point fixed so that differences between the two traces reflect only the presence or absence of the applied magnetic field.

Figure 13 extends the magnetized krypton case across the full discharge-current sweep. The three panels separate the data by cathode flow rate, and within each panel, the keeper voltage power spectral density is overlaid for every discharge current investigated at that flow. Plotting the current sweep this way makes it possible to read off, at a glance, how the oscillation spectrum evolves as the cathode is pushed from low to high emission current at fixed flow.

Figure 14 presents the analogous data set for argon at the magnetized condition used in this study. As in the krypton three-panel figure, each panel corresponds to a single cathode flow rate and overlays every discharge current run at that flow. The argon current sweep is denser than the krypton sweep at low flow because the cathode tolerates lower emission currents in argon; the mapping of current to color is preserved, so the two propellants can be read side by side.

Figure 15 isolates the effect of magnetization on argon operation. The three panels compare the magnetized and unmagnetized keeper voltage power spectral density at a discharge current of 10 A for each of the three cathode flow rates. Because only the applied magnetic field is toggled between the two traces in each panel, differences in oscillation content across the pair can be attributed to magnetization rather than to flow or current.

Discussion

This section discusses the key findings from the experimental characterization of the heaterless H9 cathode. First, the physical mechanisms driving the oscillatory behavior observed during ignition are examined. Second, the steady-state voltage-current characteristics under magnetized and unmagnetized conditions are discussed, with particular attention to the unexpected increase in voltage in the magnetized case and its implications for plasma dynamics.

Ignition oscillations

The oscillatory behavior observed during the first few minutes of ignition is consistent with repeated arc transitions and with the dynamic interaction between the discharge and the current-limited high-voltage keeper supply during the Paschen-regime heating phase. Such oscillations are not inherent to Paschen or glow discharges and can be largely eliminated by cathode conditioning and proper impedance matching between the supply and the discharge. In this phase, a high voltage applied between the cathode and keeper drives electrical breakdown of the propellant gas, producing a glow discharge that heats the emitter through ion bombardment across the cathode sheath until thermionic emission can take over [3, 10, 15]. The three-stage progression of breakdown, heating, and steady-state thermionic operation is consistent with the framework established for other heaterless designs [3, 7]. During the voltage-rise phase, electrons in the cathode cavity are accelerated by the growing electric field but cannot sustain ionization until the electron-neutral collision rate and electron energy are sufficient to trigger an avalanche at the Paschen breakdown threshold, which in the present work occurs near 905 V on krypton at 100 to 140 sccm. Upon breakdown, the discharge impedance drops sharply and the keeper voltage collapses. The voltage then rises again as the supply drives to hold the commanded current, repeating the cycle. Payman and Goebel report that low-impedance arc events during the Paschen heating phase produce transient current spikes and voltage oscillations, and that these dampen as the tantalum tube reaches thermionic emission temperatures above 2300 °C [3]. The present observations are consistent with that behavior: the oscillations persist until thermionic emission is established, after which the discharge stabilizes. Because the Paschen breakdown voltage in an HHC depends on the cathode-keeper neutral density, which is set by flow rate and cathode geometry under rarefied, non-static-pressure conditions [7], a higher ignition flow rate reduces the number of relaxation cycles before the discharge settles into a sustained arc, as evidenced in Fig. 7.

The flow-rate scan shown in Figs. 7 and 8 is consistent with the cathode operating on the low-pressure (left) branch of the Paschen curve [7]. As the neutral density in the insert volume rises with cathode flow, the electron-neutral mean free path decreases and the voltage required for breakdown drops toward the Paschen minimum. The relatively flat shoulder near 905 V observed from 100 to 140 sccm reflects a gently sloped region of the left branch for this cathode geometry, combined with the nonlinear mapping from cold-flow rate to actual insert neutral pressure under the rarefied, non-static-pressure conditions that bound the validity of a standard Paschen description in heaterless hollow cathodes [7]. The sharp drop to 795 V at 150 sccm marks the onset of the steeper descent toward the Paschen minimum. The accompanying damping of pre-breakdown chatter at higher flow is consistent with faster neutral replenishment of the insert volume between breakdown attempts.

The propellant comparison between Fig. 6 (krypton) and Fig. 9 (argon) is consistent with the same physics. Argon has a higher first-ionization potential (15.76 eV) than krypton (14.0 eV). Daykin-Iliopoulos et al. observed in a 30 A heaterless hollow cathode that argon operation required higher keeper voltage and higher emitter temperature than krypton or xenon at matched pressure, which they attribute to argon's higher ionization potential and lower ion mass requiring a higher electric field strength to maintain sufficient ionization [9]. The same mechanism is expected to raise the neutral density required to initiate breakdown, which appears in the present data as the higher ignition flow rate observed for argon (140 sccm versus 72 sccm on krypton, roughly a factor of two). Practically, this indicates that the HECCTR-class heaterless design [3] inherits a propellant-dependent minimum flow for reliable ignition, with the argon floor well above the krypton floor.

Steady-state operation

The steady-state voltage-current characteristics of the heaterless hollow cathode were characterized on krypton and argon, under magnetized and unmagnetized conditions, at three cathode flow rates (12.39, 15.89, and 22.33 sccm). At matched current and flow, the magnetized configuration sat at a higher discharge voltage than the unmagnetized configuration on both propellants, and the gap grew with discharge current and narrowed with cathode flow. At matched conditions, the argon gap was several times the krypton gap in absolute volts. Two practical limits truncated the test matrix at higher currents. On krypton, magnetized operation was stopped at 30 to 35 A, while unmagnetized operation reached 45 A, because the stainless-steel mock anode began to glow yellow, corresponding to an incandescent anode-surface temperature of approximately 1000 to 1100 °C by color, and further current was not pursued to avoid thermally compromising the ceramic standoff that isolates the mock anode from the test stand. On argon, the discharge voltage in the magnetized configuration climbed more steeply with current than on krypton, reaching 110 V at 20 A and 15.89 sccm, and the argon matrix was truncated at 20 A when the discharge voltage approached the 150 V compliance of the discharge power supply. The paragraphs below examine the most likely physical mechanism consistent with these observations and discuss the bounding caveats. The external anode geometry follows the HECCTR reference cathode of Payman and Goebel [3], on which the present cathode is based: a 56.9 mm diameter cylindrical anode positioned to reproduce a Hall-thruster-like field profile. Unlike that reference configuration, the present anode was not water-cooled, which is why it reached the yellow-glow thermal limit at the highest krypton currents; an actively cooled or resized anode is planned for future work to extend the current envelope. The relatively small anode diameter also confines neutrals in the near-anode region, which enhances local ionization and tends to lower the oscillation level, an effect expected to be most pronounced in the unmagnetized configuration; this geometric contribution should be kept in mind when interpreting the magnetized-versus-unmagnetized comparison, though it was not the variable toggled in this study.

The argon characterization reached only 20 A, a third of the 60 A design current, because the magnetized discharge voltage approached the 150 V compliance of the discharge supply and the mock anode approached its thermal limit. Operation of a high-current cathode at low fractions of its rated current can favor cold, unstable plume-mode operation, and the elevated oscillation levels observed on argon should be interpreted with this in mind. Future iterations should employ a higher-compliance discharge supply, higher cathode flow rates, and an anode sized or cooled for sustained high-current collection to extend the argon envelope toward the design current.

The physical mechanism most consistent with this observation is that the applied magnetic field increases the plasma impedance rather than easing electron transport. In this picture, the applied magnetic field enhances wave activity in the cathode plume, raising the effective (anomalous) electron collision frequency above the classical value. A higher effective collision frequency is consistent with a higher effective plasma resistivity and a steeper plasma potential gradient between cathode and anode, and therefore with a higher voltage required to drive the same discharge current. This chain is consistent with what was measured: magnetized discharge voltage higher than unmagnetized discharge voltage at matched current. Non-classical, wave-driven resistivity in magnetized cathode plumes has been reported to exceed classical values by two to three orders of magnitude in coupled-cathode Hall thruster operation [1, 11]. A related effect has been characterized in applied-field MPD thrusters, where the anode sheath voltage fall rises approximately linearly with applied magnetic field [16]. The present configuration is a standalone cathode in a mock H9 magnetic field, not a coupled cathode or an MPD thruster, so these references establish a class of mechanism that is consistent with the voltage behavior rather than a one-to-one comparison. The test operator also observed the stainless-steel mock anode surface glowing yellow during magnetized operation, which corresponds to an incandescent anode-surface temperature of approximately 1000 to 1100 °C by color and is consistent with elevated energy deposition at the anode.

The difference in the magnitude of the magnetization effect between argon and krypton follows from the same picture. Argon has a lower atomic mass than krypton and a higher first-ionization potential (15.76 eV versus 14.0 eV), so at matched discharge current and flow rate the argon discharge is expected to sit at a higher electron temperature than the krypton discharge. Daykin-Iliopoulos et al. observed this directly in a 30 A heaterless hollow cathode, where argon operation required a higher emitter temperature than krypton or xenon at matched pressure, which they attribute to argon's higher ionization potential and lower ion mass requiring a higher electric field strength to maintain sufficient ionization [9]. The same scaling of electron temperature with ionization potential and mass has been invoked to account for lighter-propellant operation of Hall thrusters [8]. A hotter electron population sits behind a thicker anode sheath because the Debye length, and therefore the characteristic sheath thickness, scales with electron temperature [1], so a larger fraction of the applied voltage is dropped in the anode sheath in argon. This interpretation is consistent with the magnetized-unmagnetized voltage gap growing more steeply on argon than on krypton at matched current and flow, and with the largest argon shifts (+ 67.5 V at 20 A and 15.89 sccm) exceeding the largest krypton shifts (+ 39.6 V at 30 A and 12.39 sccm) even though the argon sweep tops out at a lower discharge current.

Two caveats bound this interpretation. First, the configuration tested here is a standalone cathode in a mock H9 magnetic field, not a cathode coupled to an H9 thruster discharge. The shift observed in the standalone geometry is therefore not a direct prediction of how the same cathode would behave coupled to the H9, where the near-cathode field topology and the plume boundary conditions are different. Second, the quantitative partition of the voltage rise into bulk-resistivity and sheath contributions cannot be resolved without plasma diagnostics internal to the discharge. What the present data do establish is that the near-cathode field topology is a first-order lever on the operating point for HECCTR-class heaterless cathodes and should be treated as a design variable, not a boundary condition, when integrating this cathode class into Hall thrusters.

Frequency analysis

The keeper-voltage power spectral density is read here as an operating-state diagnostic. Elevated keeper peak-to-peak and oscillation content at the keeper electrode have been reported as a first indicator of transition toward plume-mode operation in hollow cathodes, which is an unstable operating regime [10]. The magnetized-versus-unmagnetized PSD pairs shown for krypton in Fig. 12 and for argon in Fig. 15 show that toggling the applied magnetic field at fixed discharge current and fixed flow shifts the spectrum. The narrow peak near 80 kHz in the magnetized krypton trace of Fig. 12 may correspond to a rotational (azimuthal) mode; the single-channel keeper-voltage measurement cannot resolve mode number or propagation direction, so this identification remains tentative. The steady-state IV result shows that the same toggle shifts the discharge voltage at fixed current. The concurrent shift of the operating-point voltage and the spectrum is most consistent with the magnetized configuration placing the cathode at a different operating state on the same hardware rather than the same operating state with additional stochastic forcing.

The current- and flow-rate sweeps at the magnetized condition (Figs. 13 and 14) indicate that the spectrum is sensitive to discharge current at a fixed flow on both propellants, with argon showing the pattern more clearly because the cathode tolerates a denser, low-current envelope on argon. In coupled magnetically-shielded cathode plumes, spectral content in this general class of cathode oscillation has been attributed to ion acoustic turbulence and to azimuthal anti-drift modes associated with enhanced electron collisionality [11]. The present configuration is a standalone cathode rather than a cathode coupled to a thruster discharge, and the keeper-voltage PSD is a single-channel measurement that does not resolve mode numbers or propagation direction, so a direct mechanism attribution is not made here. What the data do establish is that keeper-voltage PSD is a cheap, non-intrusive diagnostic of operating state for this cathode class and can flag shifts in the cathode operating state without adding intrusive diagnostics to the discharge.

Conclusion

This work produced findings in three areas: ignition, steady-state magnetization, and keeper-voltage spectra. The two central results concern steady-state magnetization. First, the applied magnetic field increases the discharge impedance rather than reducing it, as evidenced by magnetized-unmagnetized discharge-voltage gaps of up to +39.6 V (+148%) on krypton and up to +67.5 V (+159%) on argon, with the gap growing as discharge current increased and cathode flow decreased. This counterintuitive result indicates that the largely axial magnetic field downstream of the cathode does not simply funnel electrons to the anode. The most likely explanation, consistent with the external telemetry, is that magnetization raises the effective (anomalous) electron collision frequency in the plume and steepens the plasma potential gradient between cathode and anode; a contribution from an increased anode sheath voltage fall cannot be excluded without plasma diagnostics internal to the discharge. Second, the propellant's atomic mass and ionization potential significantly influence the magnitude of the magnetization effect, with the lighter argon showing a stronger voltage increase than krypton, supporting the hypothesis that less efficient energy transfer in electron-neutral collisions with lighter species leads to higher electron temperatures. Beyond the magnetization result, the ignition characterization established that reliable cold-cathode breakdown on this design is propellant-dependent: krypton required a higher cold-flow rate for sustained breakdown than a conditioned cathode, and argon required a higher flow still, consistent with its higher ionization potential. The cold-flow scan further showed the breakdown voltage falling as cathode flow increased, consistent with operation on the low-pressure branch of the Paschen curve. Finally, the keeper-voltage power spectral density was shown to be a low-cost, non-intrusive indicator of cathode operating state, shifting measurably when the applied field was toggled at fixed current and flow. These results demonstrate that the HECCTR-based heaterless H9 cathode operates repeatably and stably on both krypton and argon, and that magnetic field effects are an important design consideration for optimizing heaterless cathode performance in Hall thruster applications.

Acknowledgements
The authors thank Dr. Dan Goebel (Jet Propulsion Laboratory) for his support in the design and construction of the heaterless cathode used in this study.

Author contributions
N.B.-C. conceived the study, designed and built the experimental setup, conducted all experiments, performed the data analysis, prepared all figures and tables, and wrote the original manuscript. D.L. and M.L.R.W. reviewed and edited the manuscript and supervised the work. All authors reviewed and approved the final manuscript.

Funding
This work was supported by a NASA Space Technology Graduate Research Opportunity (Grant No. 80NSSC20K1224).

Data availability
No datasets were generated or analysed during the current study.

Code availability
Not applicable.

Declarations

Ethical approval
Not applicable.

Consent to participate
Not applicable.

Consent for publication
Not applicable.

Use of generative AI
The authors used Claude (Anthropic) to assist with citation formatting and editorial refinement of selected paragraphs. All AI-assisted content was reviewed, verified, and edited by the authors, who take full responsibility for the accuracy and integrity of the work. No AI was used to generate figures or original research findings.

Competing interests
The authors declare no competing interests.

Received: 25 April 2026 / Accepted: 9 September 2026

References

1. Goebel DM, Katz I (2008) Fundamentals of electric propulsion: Ion and Hall thrusters. Wiley, Hoboken. https://doi.org/10.1002/9780470436448
2. Lev DR, Mikellides IG, Pedrini D et al (2019) Recent progress in research and development of hollow cathodes for electric propulsion. Rev Mod Plasma Phys 3:6. https://doi.org/10.1007/s41614-019-0026-0
3. Payman AR, Goebel DM (2022) Development of a 50-A heaterless hollow cathode for electric thrusters. Rev Sci Instrum 93:113543. https://doi.org/10.1063/5.0124694
4. Goebel DM, Payman AR (2023) Heaterless 300 A lanthanum hexaboride hollow cathode. Rev Sci Instrum 94(2):023302. https://doi.org/10.1063/5.0135616

5. Lev D, Alon G, Appel L, Seeman O, Hadas Y (2017) Low current heaterless hollow cathode development overview. In: 35th International Electric Propulsion Conference
6. Vekselman V, Krasik YE, Gleizer S, Gurovich VT, Warshavsky A, Rabinovich L (2013) Characterization of a heaterless hollow cathode. J Propul Power 29(2):475–486
7. Daykin-Iliopoulos A, Gabriel SB, Golosnoy I, Kubota K, Funaki I (2015) Investigation of heaterless hollow cathode breakdown. In: 34th International Electric Propulsion Conference, IEPC-2015-193, Kobe-Hyogo, Japan
8. Linnell JA, Gallimore AD (2006) Efficiency analysis of a Hall thruster operating with krypton and xenon. J Propul Power 22(6):1402–1412. https://doi.org/10.2514/1.19613
9. Daykin-Iliopoulos AJN, Golosnoy IO, Gabriel SB, Bosi F (2019) Characterisation of a 30 A heaterless hollow cathode. In: 36th International Electric Propulsion Conference, IEPC-2019-802, Vienna, Austria
10. Becatti G, Conversano RW, Goebel DM (2021) 25,000 ignitions of a proto-flight compact heaterless lanthanum hexaboride hollow cathode. Acta Astronaut 178:181–191. https://doi.org/10.1016/j.actaastro.2020.08.037
11. Jorns BA, Cusson SE, Brown Z, Dale E (2020) Non-classical electron transport in the cathode plume of a Hall effect thruster. Phys Plasmas 27(2):022311. https://doi.org/10.1063/1.5130680
12. Hofer RR, Cusson SE, Lobbia RB, Gallimore AD (2017) The H9 magnetically shielded Hall thruster. In: 35th International Electric Propulsion Conference, IEPC-2017-232
13. Goebel DM, Watkins RM, Jameson KK (2007) LaB6 hollow cathodes for ion and Hall thrusters. J Propul Power 23(3):552–558. https://doi.org/10.2514/1.25475
14. Chapman WAJ (1972) Workshop technology, part 1, 5th edn. Edward Arnold, London
15. Baalrud SD, Scheiner B, Yee BT, Hopkins MM, Barnat E (2019) Interaction of biased electrodes and plasmas: sheaths, double layers and fireballs. arXiv:1911.06424
16. Lev D, Choueiri EY (2011) Scaling of anode sheath voltage fall in applied-field MPD thrusters. In: 32nd International Electric Propulsion Conference, IEPC-2011-222, Wiesbaden, Germany

Publisher's note